Solar Energy Materials & Solar Cells 164 (2017) 40–46

Contents lists available at ScienceDirect

Solar Energy Materials & Solar Cells

journal homepage: www.elsevier.com/locate/solmat

Efficient nanostructured quasi-single crystalline silicon solar cells by metal-catalyzed chemical etching

Qiang Wang[a,b], Chengfeng Pan[a], Kexun Chen[a], Shuai Zou[a], Mingrong Shen[a], Xiaodong Su[a,c,*]

[a] College of Physics, Optoelectronics and Energy, Collaborative Innovation Center of Suzhou Nano Science and Technology, and Jiangsu Key Laboratory of Thin Films, Soochow University, 1 Shizi Street, Suzhou 215006, China
[b] School of Electronic and Information, Nantong University, Nantong 226019, China
[c] State Key Laboratory of Silicon Materials, Zhejiang University, Hangzhou 310027, China

ARTICLE INFO

Keywords:
Quasi-single crystalline silicon solar cells
Metal-catalyzed chemical etching
Nano-texture
Parallel sub-cell model
Power conversion efficiency

ABSTRACT

Seed-assisted cast quasi-single crystalline silicon (Qsc-Si) technique allows the production of efficient, low-cost solar cells. However, most of the Qsc-Si wafers still consist of single- and multi-crystalline silicon grains, which lead to difficulties when attempting to achieve high efficiency by using conventional acid or alkali texture processes. This paper highlights the fact that nano-textured Qsc-Si solar cells can reach efficiencies ranging from 18.4% to 18.9% by using the same metal-catalyzed chemical etching technique, along with a depressed color difference. A parallel sub-cell model is proposed to explain how to enhance the performance of Qsc-Si cells.

1. Introduction

In recent years, crystalline silicon, including cast multi-crystalline (mc-Si), and Czochralski (CZ) single crystal (sc-Si), have dominated approximately 90% of the photovoltaic (PV) market [1–4]. From the viewpoint of the total cost of production, both sc-Si and mc-Si have advantages and disadvantages: costly sc-Si solar cells are efficient due to nearly perfect material quality, but suffer from serious light-induced degradation (LID) of efficiency due to B-O bonding; cost-effective mc-Si solar cells have 1–2% lower efficiencies than those of sc-Si cells because of more crystallographic defects and higher light loss [5–7].

The seed-assisted cast quasi-single crystalline silicon (Qsc-Si) technique was recently developed by carefully controlling the growth condition to grow < 100 > oriented sc-Si grains in most vertical and horizontal areas of an ingot [8–11]. Qsc-Si solar cells are expected to have efficiency close to that of sc-Si cells, due to high minority carrier lifetimes, lower grain boundaries and dislocations, while keeping the low cost and LID of mc-Si cells. It was reported that the efficiency of Qsc-Si solar cells has wide distribution, from 17.1% to 18.2%, as the ratio of sc-Si grains in the wafers varies from 50% to 100% [12–14]. However, Qsc-Si is still unpopular in the PV industry, due to two main factors: first, although it is higher in efficiency, the cost of Qsc-Si is higher than that of mc-Si. Second, most Qsc-Si wafers consist of both sc- and mc-Si grains, thus making it difficult to obtain proper texture for light trapping, and thus it reaches high efficiencies by using either conventional alkali or acid texture processes [15]. Therefore, the need to find an effective texturing technique for the efficient Qsc-Si cell is urgent.

The nanostructured black silicon with extremely low reflectivity has attracted attention due to its potential application in silicon-based solar cells [16,17]. Theoretically, the nano-texture can be treated as a density-graded or refraction-graded layer, which can smoothly connect the air and Si substrate, thus allowing it to suppress light reflection exponentially as the grade depth increases [18]. Several techniques, such as laser texturing, reactive ion etching (RIE), and metal-catalyzed chemical etching (MCCE), are attractive because various nanostructures can be formed on the surface regardless of grain orientations of Si wafers [19–24]. MCCE has been verified as a universal nano-texture technique for sc-Si and mc-Si wafers, and it is much more suitable for the current industry product line due to its low cost and stability. However, it is still a challenge to obtain a proper texture for both sc- and mc-Si grains in a Qsc-Si wafer, in an aim to achieve good cell performance, i.e., excellent light trapping ability, less color difference, and high efficiency.

In this work, the Qsc-Si solar cells with a mixture of sc- and mc-Si grains demonstrated 18.4% to 18.9% efficiencies using our well-established MCCE nano-texture process [25,26], and the results show that the cast Qsc-Si can be competitive with both CZ sc-Si and cast mc-Si.

* Corresponding author at: College of Physics, Optoelectronics and Energy, Collaborative Innovation Center of Suzhou Nano Science and Technology, and Jiangsu Key Laboratory of Thin Films, Soochow University, 1 Shizi Street, Suzhou 215006, China.
E-mail address: xdsu@suda.edu.cn (X. Su).

http://dx.doi.org/10.1016/j.solmat.2017.02.002
Received 12 November 2016; Received in revised form 23 January 2017; Accepted 1 February 2017
Available online 14 February 2017

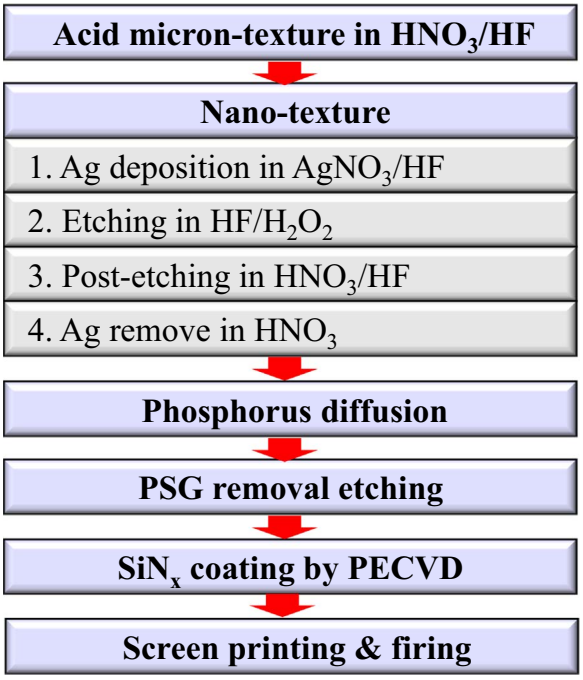

Fig. 1. Fabricating process of Qsc-Si solar cells with micron- or nano-texture.

2. Experimental

Qsc-Si wafers (p-type, 156×156×0.2 mm^3, resistivity of 1–3 Ω.cm) were provided by Zongyi New Materials Inc., China. The fabrication process of nano-textured Qsc-Si solar cell is presented in Fig. 1. First, all as-cut Qsc-Si wafers underwent nitric acid/hydrofluoric acid (HNO_3/HF) etching to remove sawn-damage layers and form proper micron-texture on the surface. Then, pre-textured Qsc-Si wafers were applied to the metal-catalyzed chemical etching (MCCE) process, as detailed elsewhere [26,27]. In brief, the above micron-textured wafers were first deposited with silver (Ag) nanoparticles, and were then etched in hydrofluoric acid/hydrogen peroxide/water (HF/H_2O_2/H_2O) solution to form a number of nano-pores on the surface. The wafers had a post-etch in HNO_3/HF solution to convert nano-pores into final nano-texture, which was immediately dipped in a 69% HNO_3 solution to remove remaining Ag nanoparticles. Finally, all nano-texture Qsc-Si wafers were assembled into cells using a standard process, including phosphorus diffusion, removal of the edge, and back *p–n* junctions, the plasma-enhanced-chemical-vapor-deposition of the SiN_x antireflection layer, and the metallization of both front and rear contacts.

PL image of Qsc-Si ingot were measured by PLI-200 (Semilab PLI-200, Hungary). The surface and cross-sectional morphologies of the silicon wafers with different textures were observed by a scanning electron microscope (SEM, Hitachi, S4800, Japan). The optical reflectance spectra were detected using a spectrophotometer with an integrating sphere (Radiation Technology D8, China). The external and internal quantum efficiencies (EQE/IQE) were measured by a quantum efficiency measuring system (QEX7, USA). The electrical performances of solar cells were characterized by IV measurement system (Berger PSL-SCD, Germany), WT2000 (Semilab WT2000, Hungary).

Table 1
Description of Qsc-Si wafers of different percentages of sc-Si grains.

Qsc-Si	sc-Si grains (%)	Lifetime (μs)	Wafer numbers
A	> 90	≦1. 5	18
B	60–90	2.45–9.32	151
C	30–60	9.32–8.35	151
D	< 30	8.35–4.00	151

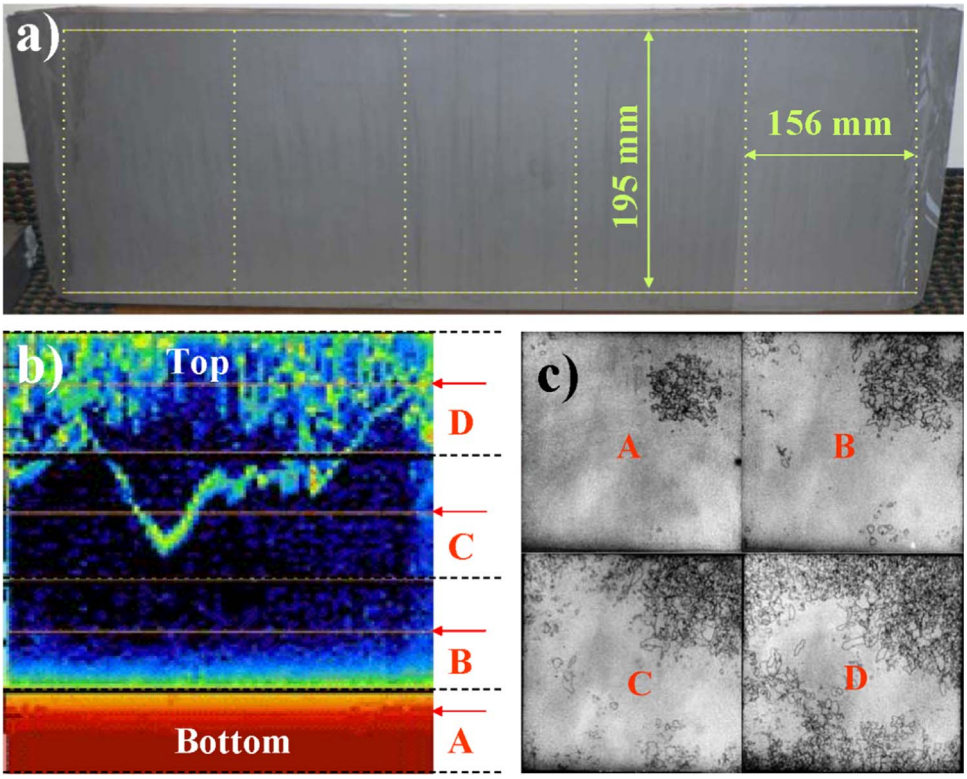

Fig. 2. a) Sectional-plane photo of an as-grown Qsc-Si ingot with a size of 800×800×248 mm^3.b) Sectional-plane PL image of a typical Qsc-Si brick with a size of 156×156×195 mm^3, cut from the center of an as-grown Qsc-Si brick. c) PL images of A, B, C, and D wafers, consisting of different proportions of sc- and mc-Si grains.

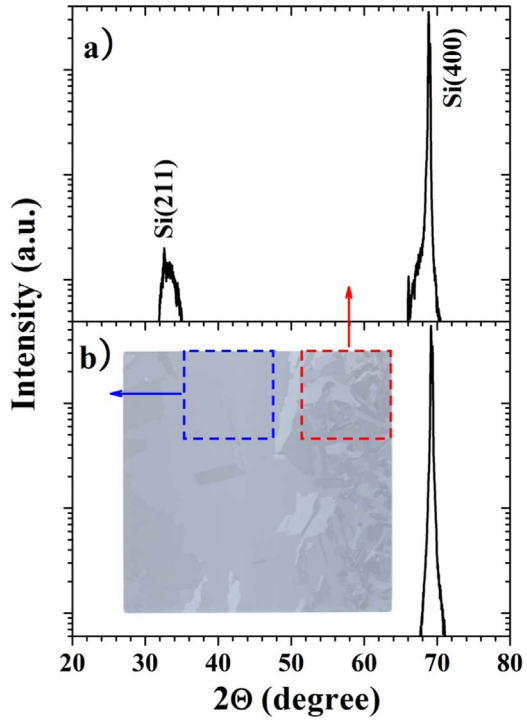

Fig. 3. XRD patterns of a) sc-Si and b) mc-Si plates, which sliced from an as-cut Qsc-Si wafer in C group. Inset: a typical wafer with two highlighted pieces for detection.

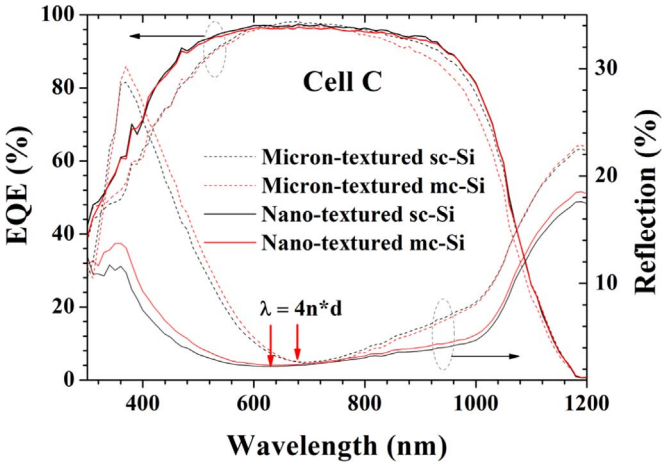

Fig. 5. EQE and reflectivity of micron- and nano-textured cell C, showing different features in sc- and mc-Si grains.

Table 2
Mean reflection and EQE statistics of sc- and mc-Si grains in cell C.

		R (%)	d (nm)	EQE (%)
sc-grain	Micron-texture	9.17	82.76	86.08
	Nano-texture	4.69	76.81	88.98
mc-grain	Micron-texture	9.48	82.93	84.62
	Nano-texture	4.13	77.32	88.51

3. Results and discussion

Four groups of Qsc-Si wafers (A, B, C, and D) were cut from the bottom to the top of a Qsc-Si ingot, as shown in Fig. 2. In Fig. 2a), the highlighted area in the sectional plane of as-grown Qsc-Si ingot (800×800×248 mm^3) has a similar morphology as sc-Si. After removing the shell, which has a very low lifetime of less than 1 μs, as-grown Qsc-Si ingot can be cut into 25 bricks with the dimensions of 156×156×195 mm^3. Fig. 2b) shows a PL image of a typical brick cut from the center part of an as-grown ingot, in which the lifetime of the minority carrier varied widely from the bottom to the top of the brick. Therefore, the brick can be classified into four zones, A, B, C, and D, according to their lifetimes, as shown in Table 1. Correspondingly, the four groups of wafers (totaling 471 pieces) were sliced from the A, B, C, and D zones in the brick. Fig. 2c) indicates that the proportion of sc-Si grains in the wafers has decreased from group A to group D. As

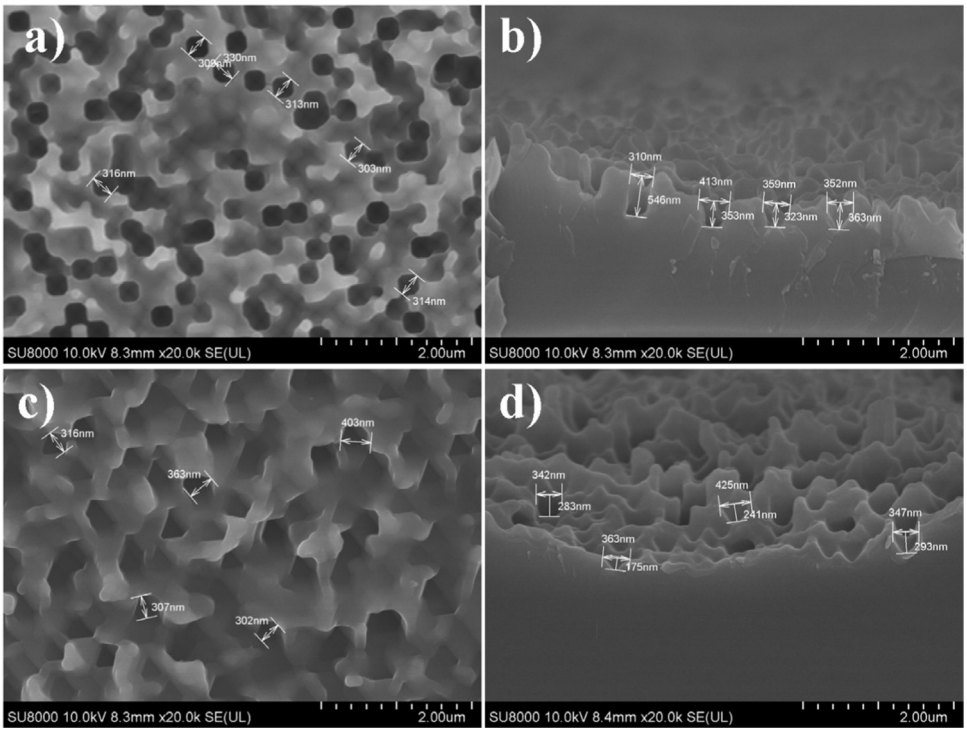

Fig. 4. Typical surface SEM images of nano-textured Qsc-Si wafers in the area of a)/b) sc-Si grain, and c)/d) mc-Si grain.

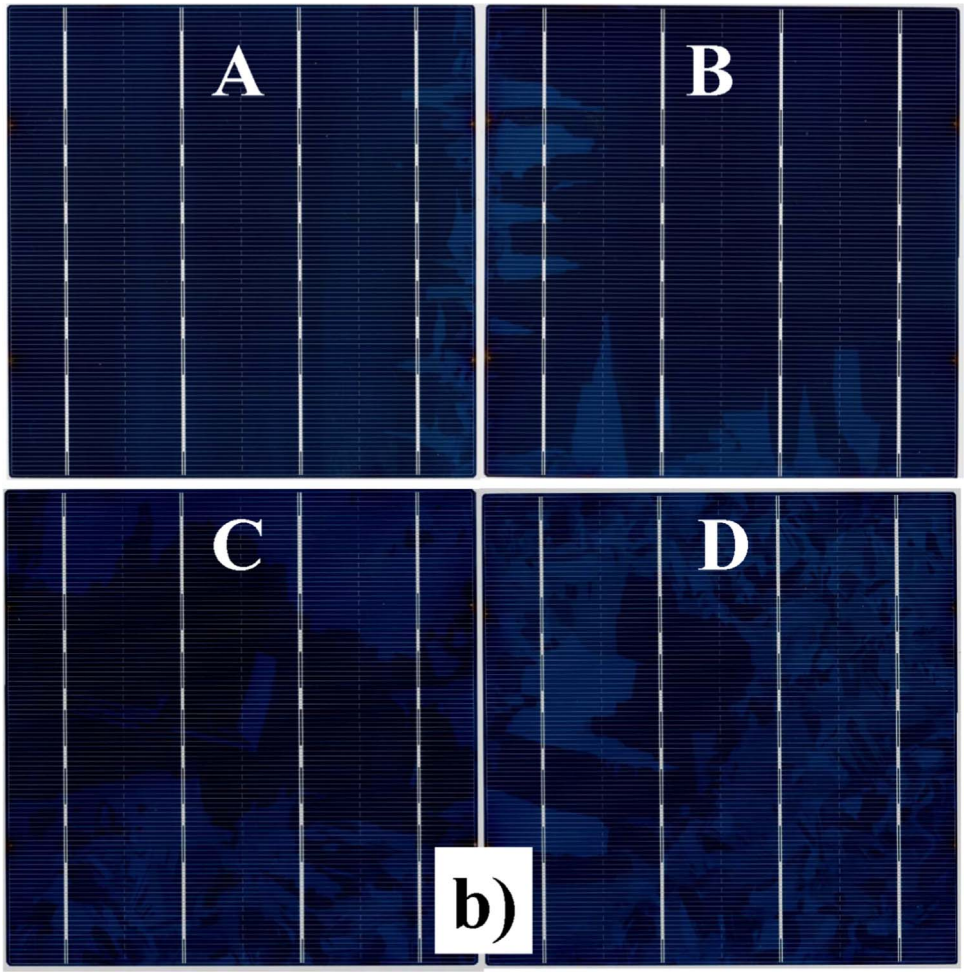

Fig. 6. Photos of Qsc-Si solar cells with different proportions of sc-Si grains, showing color differences. (Cell area 243.36 cm^2, the top Ag electrode with 91 grid lines was screen printed with PV17F Ag paste from DuPont).

Table 3
Characterizations of Qsc-Si cells with micron- and nano-textures.

Cell	Texture	V_{oc} (mV)	J_{sc} (mA cm^{-2})	R_s (Ω cm^2)	R_{sh} (kΩ cm^2)	FF (%)	η (%)
A	Micron	637.0	36.08	0.37	137.0	79.76	18.35
	Nano	634.1	36.61	0.33	154.1	80.08	18.59
B	Micron	638.5	36.19	0.39	144.1	79.84	18.45
	Nano	637.2	36.85	0.35	191.0	80.17	18.83
C	Micron	633.3	36.58	0.35	105.4	79.91	18.31
	Nano	630.6	36.58	0.35	158.2	80.12	18.48
D	Micron	624.5	35.53	0.37	183.5	79.42	17.63
	Nano	625.4	36.16	0.33	196.6	79.85	18.07

expected, wafer A has the highest proportion of sc-grains because it is nearest to the seed layer. However, the low lifetime of less than 1.5 μs implies that zone A contains many defects and impurities diffused from the crucible [27–29].

Fig. 3 shows X-ray diffraction (XRD) patterns of the two small pieces cut from a typical wafer in group C, confirming that the wafer consists of sc- and mc-Si grains, whereas sc-grains are usually of (001)-orientation. In our primary work, the Qsc-Si wafer shows a pyramidal texture in sc-Si area, but overlapped-tile texture and sharp step edges between different grains in mc-Si area under anisotropic alkali etching. If the Qsc-Si wafer was textured in separate acid and alkali etching steps, then the process becomes more complicated and expensive. Therefore, the Qsc-Si wafer with high sc-grain proportion is usually applied to an isotropic acid etching to form an oval-shape texture by sacrificing the light-trapping advantage of pyramidal texture [8,12,15, 30]. To solve this problem, four groups of Qsc-Si wafers were applied using the same MCCE process to form nano-textures, which has been verified for mc-Si wafers [26,27].

The proportion of the sc-Si grains in wafer C is close to that of the mc-Si grains; thus wafer C is representative of the verification of the MCCE process for all Qsc-Si wafers presented in this work. Fig. 4 presents the surface and cross-sectional morphologies of both sc-Si and mc-Si grains in solar cell C of a SiN_x coating (thickness, ~ 80 nm; refractive index n=2.05). Although both sc-Si and mc-Si grains had the same pre-texture and nano-texture processes applied, the morphologies and size are quite different. The nanostructure in sc-Si grains is of inverted-pyramid shapes with an open size (d) of ~360 nm and a depth (h) of ~350 nm, while it is of a declined inverted-pyramid shape with an open size of ~370 nm and a depth of ~250 nm in mc-Si grains. The results imply that sc- and mc-Si grains have different etch dynamics in

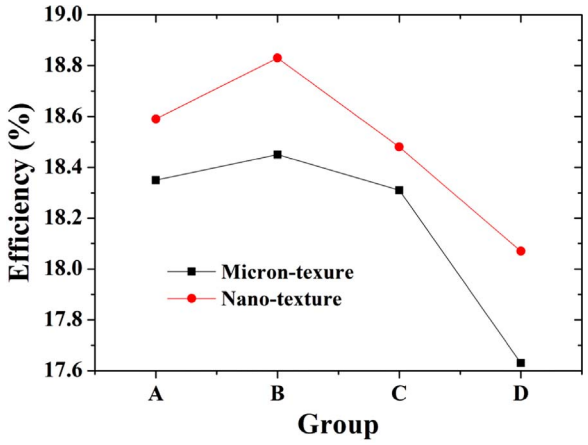

Fig. 7. Mean efficiency variation of micron- and nano-textured Qsc-Si solar cells (A, B, C, and D, 20 pieces each).

nano-texture processes, and the normal of pyramids (< 100 >) and etching rate of individual grains depend on its orientation, resulting in remarkably different microstructures between mc-Si and sc-Si wafers [26].

The nanostructure in both sc- and mc-Si grains is close to open-size, but the nanostructure depth in sc-Si grains is much deeper than that of mc-Si grains. Here, we can define an aspect ratio of $r = h/d$ to evaluate the trapping ability of the nanostructure, i.e., r=1.03 for sc-Si grains

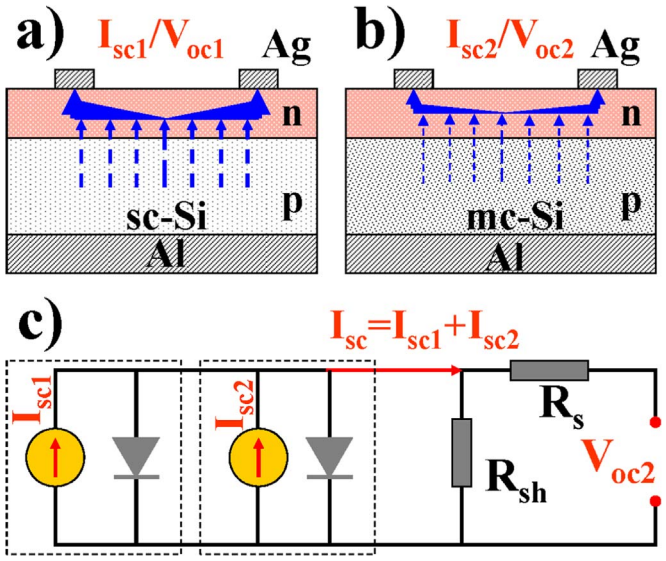

Fig. 9. Schematic illustration of a) sc-Si subcell, b) mc-Si subcell, and c) equivalent circuit of the two parallel subcells. The current flow in the subcell is indicated in blue. (For interpretation of the references to color in this figure legend, the reader is referred to the web version of this article.)

and r =0.68 for mc-Si grains. A large r means a better light trapping due to a higher gradient refraction index [18,27]. Therefore, the nano-

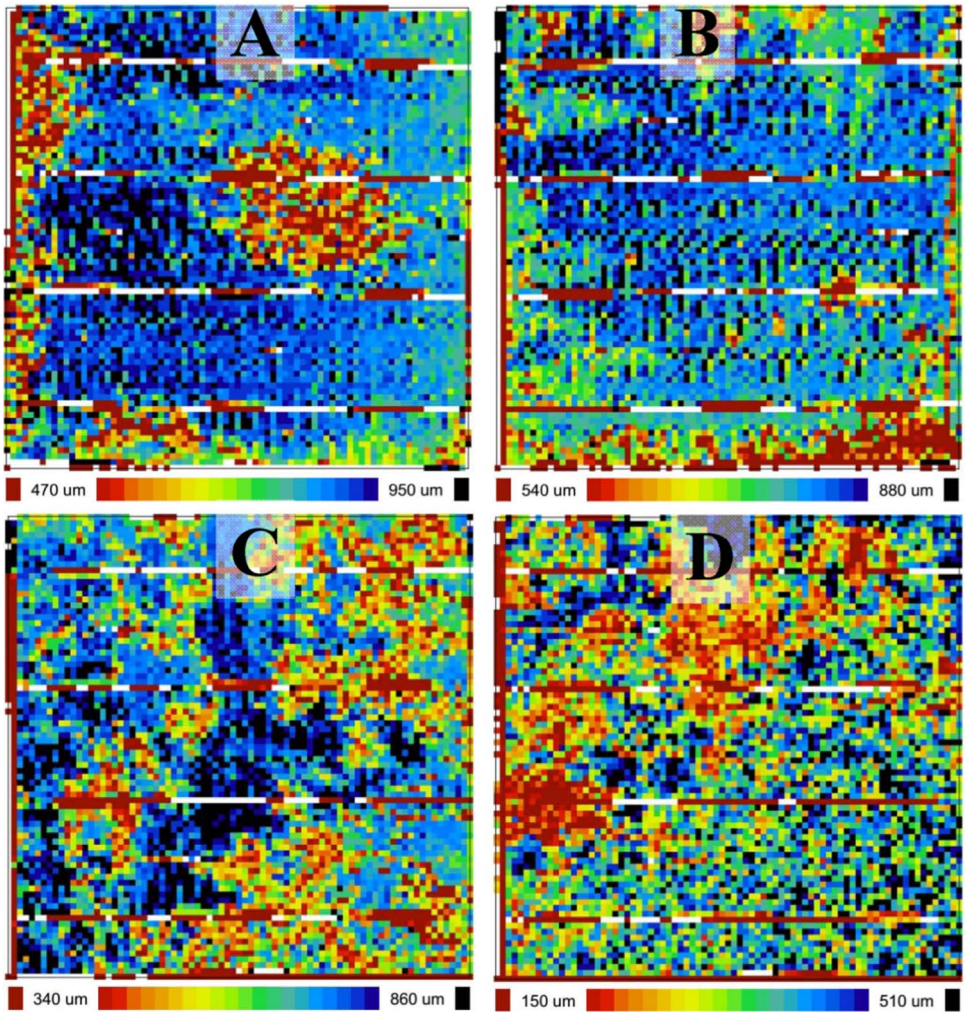

Fig. 8. Diffusion length mapping of nano-textured Qsc-Si solar cells (A, B, C, and D).

textured sc-Si grains should have better light trapping ability than that of the mc-Si ones.

Fig. 5 presents the reflectivity and external quantum efficiency (EQE) dependencies on the wavelengths of sc- and mc-Si grains in cell C with micron- and nano-textures. To give the statistics meaning, each plot presents the average values of three measured points in the cell. The mean reflectivity $\overline{R}$ (350–1050 nm) was approximately 9.17% and 9.48% for micron-textured sc- and mc-Si grains, and 4.13% and 4.45% for nano-textured sc- and mc-Si grains, respectively. Obviously, the difference of reflection values between sc- and mc-Si grains presents a color difference to the eyes. For both micron-textured and nano-textured sc-grains, the reflection difference between sc- and mc-Si grains is almost the same at ~0.3%. However, the nano-textured cell has constant and low reflection over a broad range of spectra from 560 to 800 nm. The mean reflection of nano-textured cells (4.29%) is approximately 5% lower than that of micron-textured cells (9.33%). The nanostructure has a density-graded layer that can suppress R exponentially as the grade depth increases [18,27]. It is interesting that the micron- and nano-textured cells show the differences in the lowest reflection wavelength at ~630 nm and ~680 nm, respectively. Based on the interference effect [23], a SiN_x layer with a certain thickness d is usually designed to achieve near-zero reflection at cell-interested wavelength λ,

$$n_{SiNx} * d = l/4$$

The measured refraction n_{SiNx} is 2.05. Therefore, we can calculate the thickness of SiN_x for micron-textured and nano-textured solar cells, as shown in Table 2. The thinner d of nano-textured cells implies that its nanostructure surface is larger than that of micron-textured cells.

EQE results show that the sc-grains in both micron- and nano-textured cells have higher values than mc-grains over whole visible spectra. As expected, the spectral response of nano-textured grains is superior to micron-textured grains in short wavelengths (350–600 nm) as well as in long wavelengths (800–1050 nm). The over-nanostructured texture means that there are a great number of carrier recombination centers in the cell's surface, thus deteriorating the cell's performance. In our case, nano-textured cells show a great EQE improvement compared to micron-textured cells, mainly because the nano-texture with the large opening size is easy passivated by the SiN_x coating [26].

The above results provided typical scenery for the Qsc-Si wafers and cells, especially the different features for sc- and mc-Si grains. Certainly, an ~0.3% reflection difference among sc- and mc-Si grains is acceptable, and the large color differences in the initial wafers were depressed after the MCCE process for four typical cells (A, B, C, and D), as shown in Fig. 6. Both sc- and mc-Si grains in each group have differences in proportion, shape, reflection, and EQE, which depends on the number of defects, such as crystalline orientation, amount of dislocation, etc. Nevertheless, the characteristics of the A, B, C, and D cells with micron- and nano-textures obtained from I–V measurement can give more useful information, and the mean parameters (20 pieces each) are detailed in Table 3.

Cell parameters, such as open-circuit voltage (V_{oc}), short-circuit current density (J_{sc}), series resistance (R_s), shunt resistance (R_{sh}), and filling factor (FF), vary greatly from one cell to another due to their sc- and mc-grains. To simplify the discussion, the mean efficiency of each group is plotted in Fig. 7. Both curves of micron- and nano-textured cells have same tendency of efficiencies, i.e., B > A > C > D; meanwhile, the curve of nano-textured cells is lifted entirely, but the efficiency of each group is improved more or less, i.e., 0.15–0.45%.

Although cell A had the highest sc-grain proportion, its efficiency is ~0.24% lower than that of group B. Assuming the surface of all the cells are in good passivation, the quality of silicon bulk determines the performance of cells [31]. Fig. 8 gives the diffusion length (L_d) mapping of four cells with nano-textures by using WT2000, and the mean L_d of the minor carrier is 785.07 μm, 745.72 μm, 636.06 μm, and 343.32 μm for A, B, C, and D, respectively. It is easy to distinguish the sc- and mc-Si grains in the cells of A, C, and D, because mc-Si grains have low L_d. However, cell B has an almost uniform distribution of L_d, which implies that both sc- and mc-Si grains have similar qualities.

To understand the electric properties of Qsc-Si cells, which feature a mixture of sc- and mc-Si grains, we constructed a simple model of parallel subcells as shown in Fig. 9. As indicated in Fig. 2, the size of mc-Si grains is greater than 5 mm. In our case, the front surface of the cell was covered by a pattern of 91 AG grid fingers, and the distance between two Ag fingers is less than 2 mm. From the viewpoint of circuits, a cell can be treated as a number of subcells connected in parallel. Fig. 9a) and b) schematically indicate two subcells, presuming both I_{sc1} and V_{oc1} in the sc-Si sub-cell are larger than I_{sc2} and V_{oc2} in the mc-Si one, respectively. As shown in Fig. 9c), the total I_{sc} of two parallel subcells is the sum of I_{sc1} and I_{sc2}, but the V_{oc} is limited by the low value of V_{oc1} and V_{oc2}. Although sc-Si grains consist of very high L_d (~950 μm), the lowest L_d value of mc-Si grains in cell A is only ~470 μm (~540 μm in cell B), and the low V_{oc} of mc-Si subcells suppresses the whole cell's performance. The parameters presented in Table 3 strongly support this deduction. Therefore, the performance of Qsc-Si cells, especially the V_{oc}, is actually determined by those subcells with the lowest electrical properties. We believe that the high efficiency in cell B is mainly due to the uniform quality in the whole cell.

Unfortunately, the research and development of Qsc-Si was nearly discontinued a few years ago in many PV companies due to the drawbacks, which we have already concluded in the paper. Since the Qsc-Si ingot studied in this paper was produced two years ago, and may no longer be a superior material to the current mc-Si ingot, the study's results still have a significant impact on further studies regarding fabricating high-quality Qsc-Si ingots, in which the quality of mc-Si grains and the proportion of sc-grains are equally important for the final properties of cells.

4. Conclusions

Qsc-Si wafers were nano-textured successfully using a metal-catalyzed chemical etching technique. The efficiencies of nano-textured cells were improved, in a range from 18.4–18.9%, due to the diverse qualities of the wafers from the bottom to the top of a Qsc-Si ingot, and the color difference in the Qsc-Si cells was depressed. A parallel subcell model was proposed to explain the performance of the Qsc-Si cell, which was mainly limited by the worst subcell. Nevertheless, the results showed that the performance of Qsc-Si solar cells was better than that of traditionally cast mc-Si solar cells (efficiency=18%). The further improvement of Qsc-Si cell efficiency can be achieved by not only increasing the proportion of sc-Si grains but also optimizing the quality and uniformity of both sc- and mc-Si grains.

Acknowledgments

This work was supported by the Key University Science Research Project of Jiangsu Province under Grant No. 16KJA140002 and 15KJA140003, the National Natural Science Foundation of China under Grant No. 51672183, the Special Fund for the Transformation of S&T Achievements of Jiangsu province under Grant No. BA2015045, and the Priority Academic Program Development of Jiangsu Higher Education Institutions (PAPD).

References

[1] H.J.J. Yu, N. Popiolek, P. Geoffron, Solar photovoltaic energy policy and globalization: a multiperspective approach with case studies of Germany, Japan, and China, Prog. Photovolt.: Res. Appl. 24 (2016) 458–476.
[2] Y.G. Tao, V. Upadhyaya, C.W. Chen, A. Payne, E.L. Chang, A. Upadhyaya, A. Rohatgi, Large area tunnel oxide passivated rear contact n-typeSi solar cells with 21.2% efficiency, Prog. Photovolt.: Res. Appl. 24 (2016) 830–835.
[3] T. Kinoshita, D. Fujishima, A. Yano, A. Ogane, S. Tohoda, K. Matsuyama, Y.

Nakamura, N. Tokuoka, H. Kanno, H.M. Sakata, M. Taguchi, The approaches for high efficiency HIT™ solar cell with very thin (< 100μm) silicon wafer over 23%, in: Proceeding of the 26th EU-PVSEC, Hamburg 871-874, 2011.
[4] M.A. Green, The passivated emitter and rear cell (PERC): from conception to mass production, Sol. Energy Mater. Sol. Cells 143 (2015) 190–197.
[5] J. Lindroos, H. Savin, Review of light-induced degradation in crystalline silicon solar cells, Sol. Energy Mater. Sol. Cells 147 (2016) 115–126.
[6] R.B. Ganesh, B. Ryningen, M. Syvertsen, E. Øvrelid, I. Saha, H. Tathgar, G. Rajeswaran, Growth and characterization of multicrystalline silicon ingots by directional solidification for solar cell applications, Energy Procedia 8 (2011) 371–376.
[7] W.C. Ma, G.X. Zhong, L. Sun, Q.H. Yu, X.M. Huang, L.J. Liu, Influence of an insulation partition on a seeded directional solidification process for quasi-single crystalline silicon ingot for high-efficiency solar cells, Sol. Energy Mater. Sol. Cells 100 (2012) 231–238.
[8] Y. Miyamura, H. Harada, K. Jiptner, S. Nakano, B. Gao, K. Kakimoto, K. Nakamura, Y. Ohshita, A. Ogura, S. Sugawara, T. Sekiguchi, Advantage in solar cell efficiency of high-quality seed cast mono Si ingot, Appl. Phys. Exp. 8 (2015) 062301.
[9] X.F. Qi, W.H. Zhao, L.J. Liu, Y. Yang, G.X. Zhong, X.M. Huang, Optimization via simulation of a seeded directional solidification process for quasi-single crystalline silicon ingots by insulation partition design, J. Cryst. Growth 398 (2014) 5–12.
[10] D.L. Hu, S. Yuan, L. He, H.R. Chen, Y.P. Wan, X.G. Yu, D.R. Yang, Higher quality mono-like cast silicon with induced grain boundaries, Sol. Energy Mater. Sol. Cells 140 (2015) 121–125.
[11] Q.H. Yu, L.J. Liu, W.C. Ma, G.X. Zhong, X.M. Huang, Local design of the hot-zone in an industrial seeded directional solidification furnace for quasi-single crystalline silicon ingots, J. Cryst. Growth 358 (2012) 5–11.
[12] G. Zhong, Q.H. Yu, X.M. Huang, L.J. Liu, Performance of solar cells fabricated from cast quasi-singlecrystalline silicon ingots, Sol. Energy 111 (2015) 218–224.
[13] N. Stoddard, R. Sidhu, J. Creager, S. Dey, B. Kinsey, L. Maisano, C. Phillips, R. Clark, J. Zahler, Evaluating BP Solar'sMONO2™ material lifetime and cell electrical data, in: Proceedings of the IEEE Photovoltaic Specialists Conference 001163-001168, 2009.
[14] V. Prajapati, E. Cornagliotti, R. Russell, J.M. Fernadez, R.F. Clark, N. Stoddard, P. Choulat, J. John, High efficiency industrial silicon solar cells on silicon MONO2 ™ cast material using dielectric passivation and local BSF, in: Proceedings of the 24th European Photovoltaic Solar Energy Conference, Hamburg 1171–1174, 2009.
[15] X. Gu, X.G. Yu, K.X. Guo, L. Chen, D. Wang, D.R. Yang, Seed-assisted cast quasi-single crystalline silicon for photovoltaic application: towards high efficiency and low cost silicon solar cells, Sol. Energy Mater. Sol. Cells 101 (2012) 95–101.
[16] R. Yu, Q.F. Lin, S.F. Leung, Z.Y. Fan, Nanomaterials and nanostructures for efficient light absorption and photovoltaics, Nano Energy 1 (2012) 57–72.
[17] Z.P. Huang, G. Nadine, P. Werner, J. de Boor, U. Gösele, Metal-assisted chemical etching of silicon: a review, Adv. Mater. 23 (2011) 285–308.
[18] H.C. Yuan, V.E. Yost, M.R. Page, P. Stradins, D.L. Meier, H.M. Branz, Appl. Phys. Lett. 95 (2009) 123501.
[19] T.H. Her, R.J. Finlay, C. Wu, S. Deliwala, E. Mazur, Microstructuring of silicon with femtosecond laser pulses, Appl. Phys. Lett. 73 (1998) 1673.
[20] J. Yoo, G. Yu, J. Yi, Large-area multicrystalline silicon solar cell fabrication using reactive ion etching (RIE), Sol. Energy Mater. Sol. Cells 95 (2011) 2–6.
[21] F. Toor, H.M. Branz, M.R. Page, K.M. Jones, H.C. Yuan, Multi-scale surface texture to improve blue response of nanoporous black silicon solar cells, Appl. Phys. Lett. 99 (2011) 103501.
[22] S. Koynov, M.S. Brandt, M. Stutzmann, Black multi-crystalline silicon solar cells, Phys. Stat. Sol. (RRL) 1 (2007) R53.
[23] S. Koynov, M.S. Brandt, M. Stutzmann, Black nonreflecting silicon surfaces for solar cells, Appl. Phys. Lett. 88 (2006) 203107.
[24] S. Bastide, N. Quang, R. Monna, C. Lévy-Clément, Phys. Status Solidi C. 6 (2009) 1536.
[25] X.Y. Ye, S. Zou, K.X. Chen, J.J. Li, J. Huang, F. Cao, X.S. Wang, L.J. Zhang, X.F. Wang, M.R. Shen, X.D. Su, 18.45%-efficient multi-crystalline silicon solar cell with nano-scale pseudo-pyramid texture, Adv. Funct. Mater. 24 (2014) 6708–6716.
[26] F. Cao, K.X. Chen, J.J. Zhang, X.Y. Ye, J.J. Li, S. Zou, X.D. Su, Next-generation multi-crystalline silicon solar cells: diamond-wire sawing, nano-texture and high efficiency, Sol. Energy Mater. Sol. Cells 141 (2015) 132–138.
[27] G.X. Zhong, Q.H. Yu, X.M. Huang, L.J. Liu, Influencing factors on the formation of the low minority carrier lifetime zone at the bottom of seed-assisted cast ingots, J. Cryst. Growth 402 (2014) 65–70.
[28] I. Guerrero, V. Parra, T. Carballo, A. Black, M. Miranda, D. Cancillo, B. Moralejo, J. Jiménez, J. Lelièvre, C. del Cañizo, About the origin of low wafer performance and crystal defect generation on seed-cast growth of industrial mono-like silicon ingots, Prog. Photovolt.: Res. Appl. 22 (2014) 923–932.
[29] Y. Zhang, Z. Li, Q. Meng, Z. Hu, L. Liu, Distribution and propagation of dislocation defects in quasi-single crystalline silicon ingots cast by the directional solidification method, Sol. Energy Mater. Sol. Cells 132 (2015) 1–5.
[30] T. Kaden, K. Petter, R. Bakowskie, Y. Ludwig, R. Lantzsch, D. Raschke, S. Rupp, T. Spiess, Analysis of mono-cast silicon wafers and solar cells on industrial scale, Energy Procedia 27 (2012) 103–108.
[31] A. Jouini, D. Ponthenier, H. Lignier, N. Enjalbert, B. Marie, B. Drevet, E. Pihan, C. Cayron, T. Lafford, D. Camel, Improved multicrystalline silicon ingot crystal quality through seed growth for high efficiency solar cells, Prog. Photovolt.: Res. Appl. 20 (2012) 735–746.